AIP Advances

Solving magnetic induction heating problem with multidimensional Fredholm integral equation methods: Alternative approach for optimization and evaluation of the process performance

Cite as: AIP Advances **12**, 105110 (2022); https://doi.org/10.1063/5.0100480
Submitted: 07 June 2022 • Accepted: 13 September 2022 • Published Online: 17 October 2022

J. Rak and J. Tucek

Solving magnetic induction heating problem with multidimensional Fredholm integral equation methods: Alternative approach for optimization and evaluation of the process performance

Cite as: AIP Advances 12, 105110 (2022); doi: 10.1063/5.0100480
Submitted: 7 June 2022 • Accepted: 13 September 2022 •
Published Online: 17 October 2022

J. Rak[a)] and J. Tucek

AFFILIATIONS

University of Pardubice, Faculty of Electrical Engineering and Informatics, Studentska 95, 532 10 Pardubice, Czech Republic

[a)]Author to whom correspondence should be addressed: josef.rak@upce.cz

ABSTRACT

Induction heating is a frequently used technology in both fundamental and applied research. It is heavily exploited in the industry for processing materials by heat treatments. In addition, it is viewed as a promising tool in medicine, particularly as a part of therapeutic strategies for treating cancer diseases. Thus, in order to optimize (i.e., enhance and tune) the performance of the induction heating process, several aspects must be considered, including the design of the magnetic coils, features of the magnetic fields applied, coupling of magnetic and thermal fields, and the material's characteristics. To tackle this complex problem, numerical mathematical models are often used. The results of which can help in understanding the role of the various parameters on the performance of the induction heating. Here, we present an alternative mathematical approach to solve the induction heating problem using Fredholm integral equations of the second kind with a singular kernel. To reduce the computation time, the Nyström method has been adopted. As the kernel function shows a singularity, a singularity subtraction has been involved in the developed mathematical procedure. Furthermore, the error features of the Nyström method with the singularity subtraction have been described, and convergence conditions of the proposed computational algorithm have been thoroughly identified. Although special conditions for the kernel function and the integration rule are needed, the method shows lower computing times, competing well with those of traditional finite-element based routines. The applicability of the developed methodology is demonstrated for the simulation of induction heating the body of a metal object.

I. INTRODUCTION

Induction heating is a physical process of heating the electrically conducting materials (especially, of a metallic character) upon exposing them to an alternating (AC) magnetic field inside a coil.[1] The time rate of change in magnetic flux, enclosed by a defined path, then promotes the creation of an electromotive force around the closed path, producing a flow of electrical current. This phenomenon is known as electromagnetic induction, which was discovered by Michael Faraday in 1831. In other words, when the rapidly changing magnetic field enters a conductor, a current is generated inside the material called eddy currents. The flow of eddy currents causes the emergence of heat due to the resistance behavior of the material, often referred to as Joule heat.[1] In addition, if a material is of ferromagnetic and/or ferrimagnetic nature (e.g., iron, cobalt, and nickel), its magnetic response shows a hysteresis when placed inside the AC magnetic field. As a result, heat is generated through hysteresis losses.[2] Thus, when describing the heating effects of the AC magnetic field in an object, the role of Joule heat and hysteresis losses should be considered, and their contributions should

be evaluated before the construction of a particular mathematical model.

Heating materials with AC magnetic fields are often viewed as very advantageous, as the heat is generated inside of them without a need to involve external heat sources. Moreover, induction and/or magnetic hysteresis loss heating is very rapid and effective compared to traditional methods using processes based on heat conduction, convection, and radiation. Two types of induction heating processes are recognized, i.e., stationary induction heat treatment and moving induction heat treatment.[3,4] In particular, both induction heating approaches have found several applications in various industrial fields, such as metallurgy (i.e., processing of metals and their alloys), the semiconductor industry (i.e., Czochralski crystal growth and zone refining), the processing of refractory materials, and, recently, the heat treatment of plastics in injection molding machines.[1,5–7] Induction heating provides targeted heating of an object, including surface hardening, melting, brazing, soldering, and heating to fit.

Besides the design of the coil (i.e., diameter, shape, and number of turns), the efficiency of induction heating is primarily given by the frequency of the current flowing in the coil that produces the AC magnetic field; the frequency used generally depends on the size of the object, the type of the material, and the coupling interaction between the coil and the heated object.[1] Moreover, the frequency-dependent penetration depth has been identified as one of the crucial parameters, governing the heating process. It is known that the amount of induced eddy currents in a material decreases dramatically from its surface. Thus, a reference depth d with effective eddy currents-carrying layers can be defined and is, in a case of a solid round bar, given as $d = 5000\sqrt{\frac{\rho}{\mu f}}$, where ρ is the resistivity of a material, μ represents its relative magnetic permeability, and f denotes the frequency of the AC field.[8] If a is a diameter of an object, the heating efficiency is found to show a maximum when $\frac{a}{d}$ reaches 4.[8] This corresponds to a critical operating frequency of the AC field, to which the heated material is exposed. While a further increase in f does not bring any improvements, operation below the critical frequency significantly lowers the heating efficiency due to a substantial cancelation of the eddy currents. For materials with self-sustainable magnetism (i.e., showing ferromagnetism and/or ferrimagnetism), the heating efficiency can be dramatically enhanced due to hysteresis and the emergence of the so-called microscopic eddy currents.[9] These stem from the interactions between magnetic domain walls and the microstructure during the changing magnetization of the sample. Thus, conducting materials with high magnetic permeability (in the range from 100 to 500) are highly demanded application reasons, especially to transfer heat to treated objects. In this context, the concept of magnetic heating has been found very promising in biomedical fields, more specifically in the therapeutical approaches of magnetically assisted hyperthermia for cancer treatment.[10–13] The heat generated due to hysteresis losses of single-domain magnetic nanoparticles and/or their superparamagnetic relaxation in AC magnetic fields is used to cause cancer cell necrosis.

Up until now, several mathematical models have been developed and constructed to describe the heating phenomenon induced by the AC magnetic field.[1] Most of them address only the case of Joule heat by eddy currents, with little attention to the effects of the hysteresis losses. In general, induction heating is a very complex nonlinear and nonstationary problem, involving interactions of several fields among which electromagnetic field, temperature field, and the field of thermoelastic displacements have been identified to play a significant role.[14] The modeling frequently relies on the computation of the magnetic vector potential, which is implemented in many available commercial codes, such as ANSYS, OPERA, and FLUX.[1,8,15,16] However, in cases of complicated geometrical structures and spatially uneven dimension ratios, the numerical solutions can significantly differ from experimental observations.

To model the induction heating problems, equations of the electromagnetic and thermal fields, which are coupled via the material's properties, are numerically solved in a chosen approximation. Most often, finite element computational algorithms that have been adjusted for a particular system are used; for example, Wang *et al.*[4] proposed a finite element procedure with a remesh scheme for the simulation of moving induction heat treatment issues. The results were compared with analytical solutions obtained for magnetic vector potential and temperature distributions derived from Green's function methods, proving validation of the proposed simulation approach of induction heating. Later, Ludtke and Schulze[17] developed a numerical model for the calculation of three-dimensional eddy currents and the heating process. With the finite element methods, they solved a set of Maxwell's equations together with Fourier's heat-conduction equation, considering the dependence of the material's properties on a temperature and magnetic field. Despite a relatively good match between the numerical and experimental results, the computing time was found to be very long in terms of an effective realization of the optimization processes. Furthermore, Nerg *et al.*[18] used a finite element method on coupled electromagnetic and thermal fields (i.e., Maxwell and Fourier–Kirchhoff equations) for the simulation of an induction heating system. In the suggested model, they numerically evaluated the load impedance during the heating cycle, which was then used for the description of the whole induction heating device, including the power supply, control system, load, and the impedance matching circuit. In the work by Kawaguchi *et al.*,[19] a three-dimensional finite element approach, involving the coupling of heat conduction and induced eddy currents, has been proposed, considering the relationship between the magnetic flux density, the magnetic permeability, and temperature. The numerical results correlated well with those measured experimentally, proving a significant role of the temperature dependence of the magnetic permeability in designing more efficient induction heating devices. Mach *et al.*[20] presented a fully adaptive higher-order finite element method for solving the coupled induction heating model, consisting of two partial differential equations for the distributions of the magnetic and temperature fields. The computational results were then exploited for an optimized design of a device for maximizing the heating performance for nonmagnetic billets, rotating in a static magnetic field. Furthermore, Chovan and Slodička[21,22] used a coupled system of Maxwell's equations with a nonlinear heat equation to model the induction heat process. Joule heating and electrical conductivity acted as coupling quantities between the electromagnetic and thermal equations. Using Rothe's method for energy estimates, a global mathematical solution was found to exist, explaining, in particular, hardening caused by induction heating. Similarly, in the work by Gürlebeck *et al.*,[23] magnetic induction heating has been treated as a coupled

numerical problem. However, involving the finite difference method together with the discrete potential theory. More specifically, the constructed model merged a system of Maxwell and heat equations with the formulation of the Laplace equation for the magnetic potential in the exterior domain. Moreover, nonlinear boundary conditions applied to the heat equation, transmission conditions, and asymptotic conditions imposed on the magnetic potential have been all introduced to simulate the induction heating process more effectively, although on a discrete level. Recently, Fu *et al.*[24] have developed a multiphysics analysis protocol within the COMSOL finite element environment, allowing the inclusion of the electromagnetic field, eddy current field, and temperature field in the induction heating process. This multi-field coupling model was then applied to a simulation of rapid internal heating occurring in carbon fiber reinforced polymer composite materials, providing clarification of the coupling and distribution rules for the electromagnetic-eddy current field within the induction process. Cui *et al.*[25] theoretically and experimentally addressed a new strategy of magnetic heating known as the focused induction heating (FIH) method. Within the COMSOL Multiphysics simulation platform, the magnetic and temperature fields using Maxwell's equations and transient heat transfer equation, respectively, have been computed using coupled numerical procedures, which have been found to provide a theoretical basis and practical guidance for the design and optimization of FIH techniques. Alternatively, on the theoretical level, magnetic induction heating has been described with eddy current equations coupled, with respect to the energy balance, with the heat equation and the kinetic phase transition.[26] Due to the nonlinearities in the model, a time discretization was introduced; a convergence and weak solution to the modeled problem were both found applying Rothe's method and the theory of monotone operators.

As already mentioned above, the hysteresis response is often omitted when modeling and simulating magnetic induction heating. Nevertheless, some efforts have already been described in the literature; for example, a robust model of the magnetic heating phenomenon, including a temperature dependent hysteresis curve of a ferromagnetic material, has been presented in the study by Geza *et al.*[27] They considered the magnetic vector potential and electric scalar potential to describe the electromagnetic part of the heat induction problem, heat transfer equation to model the Joule term, and the fictitious time-independent material response, effectively linearized, to account for the nonlinear magnetic phenomena typical for magnetically ordered substances. Adopting the finite element computational method, the simulation results showed a sensitivity of the proposed model to slight variations in the magnetic features of a ferromagnetic material, such as the Curie temperature, fully in accordance with the experimental observations. The nonlinear hysteresis behavior and associated heat evolution have been treated in a different manner in the work by Roppert *et al.*[28] With the proposed approach, they transformed the eddy current problem into the frequency domain, with a harmonic balancing scheme used for the magnetic hysteresis of a material. In the steady-state domain, the solution showed a good convergence, significantly decreasing the overall computational complexity of the magnetic induction heating process in the ferromagnetic materials.

In this work, we introduce an alternative approach for the solution to the induction heating problem. The method is based on the adoption of Fredholm integral equations of the second kind with a singular kernel. which is used to represent the Joule losses generated during the inducting heating process. Contrary to the frequently applied methods of solving a system of linear equations with fully populated matrices, integrals in each element of the matrix are calculated. To reduce the computation time, the Nyström method has been introduced. Due to the kernel function singularity, a singularity subtraction has been considered. In this context, we have described the error features of the Nyström method with the singularity subtraction and identified the convergence conditions of the proposed computational algorithm. Although special conditions for the kernel function and the integration rule are needed, the method shows lower computing times, well competing with those of traditional finite-element based routines.

II. MATHEMATICAL MODEL

The equation describing eddy currents of density in the induction heating process can be written as a special Fredholm integral equation of the second kind with singular kernel[29] for the function $y(x)$ of m variables, i.e.,

$$\lambda y(x) - \int_D k(x,t)y(t)dt = f(x), x \in D, \lambda \neq 0, \tag{1}$$

where $D \subset \mathbb{R}^m$ is closed, bounded, and connected set, $\mathbb{R}$ is a set of real numbers, $x, t \in D$, $\lambda \in \mathbb{R}$, and $f(x)$ is the continuous function of m variables. The function $k(x,t)$ is called the kernel function and is assumed to be an integrable function of a variable t all $x \in D$. However, the function is singular when $x = t$. The example of such a singularity is

$$k(x,t) = r^{-1}(x,t), \tag{2}$$

where $r(x,t)$ is the Euclidean distance of x and t. As we will see in the further section, such an example covers also the integral equation for eddy currents of density in the induction heating process. If we define operator $\mathscr{K}$ as

$$\mathscr{K} y(x) = \int_D k(x,t)y(t)dt, \tag{3}$$

then we can apply operator calculus for proving the existence and the uniqueness of the solution of Eq. (1). We need two conditions.[29] The first is the compactness of operator $\mathscr{K}$ on space $\mathscr{C}(D)$ (space of continuous function on D). Such an operator defined by Eq. (3) with the kernel function defined by Eq. (2) can be proved to be compact for $D \subset \mathbb{R}^m$ if $m = 1, 2, 3$.[29] The second condition implies from the Fredholm alternative. The number $\lambda \neq 0$ cannot be an eigenvalue of the operator $\mathscr{K}$.[29]

III. NYSTRÖM METHOD

The idea of the Nyström method involves the substitution of the integral by a numerical integration rule. However, a problem arises here. When $x = t$, the function $k(x,t)$ defined by Eq. (2) is singular. Thus, the singularity needs to be subtracted from Eq. (1). This technique was described in detail in a book by Kantorovich and Krylov.[30] After the singularity subtraction, Eq. (1) changes to

$$\left[\lambda - \int_D k(x,t)dt\right]y(x) - \int_D k(x,t)[y(t) - y(x)]dt = f(x). \quad (4)$$

In the second integral of Eq. (4), the function $k(x,t)$ can be approximated by a non-singular function $k_n(x,t)$, which is identical to $k(x,t)$ outside the certain neighborhood of $x = t$. We get

$$\left[\lambda - \int_D k(x,t)dt\right]y(x) - \int_D k_n(x,t)[y(t) - y(x)]dt = f(x). \quad (5)$$

Then, $k_n(x,t)[y(t) - y(x)]$ can be integrated numerically as

$$\int_D k_n(x,t)[y(t) - y(x)]dt = \sum_{j=1}^{n} w_j k_n(x,x_j)[y(x_j) - y(x)], \quad (6)$$

where x_j are node points and w_j are weights of numerical integration rule. If we replace the right integral in Eq. (5) by Eq. (6) and if we substitute the integration rule node points x_i to x, we get a system of linear equations given as

$$\left[\lambda + \sum_{j=1,j\neq i}^{n} w_j k_n(x_i,x_j) - \int_D k(x_i,t)dt\right]y_n(x_i) - \sum_{j=1,j\neq i}^{n} w_j k_n(x_i,x_j)y_n(x_j) = f(x_i). \quad (7)$$

The value $y_n(x_i)$ is a numerical solution of $y(x)$ at the integration rule node points x_i. To obtain a numerical solution at other points $x \in D$, we can use the formula by Kantorovich and Krylov,[30] i.e.,

$$y_n(x) = \frac{f(x) + \sum_{j=1}^{n} w_j k_n(x,x_j)y_n(x_j)}{\lambda + \sum_{j=1}^{n} w_j k_n(x,x_j) - \int_D k(x,t)dt}. \quad (8)$$

Formulas (7) and (8) contain improper integral,

$$\int_D k(x,t)dt. \quad (9)$$

Since $k(x,t)$ was assumed to be the integrable function of the variable t for all $x \in D$, the integral defined by Eq. (9), in Eqs. (7) and (8), can be computed analytically or by a special integration rule. In the one-dimensional case, the construction of approximating function $k_n(x,t)$ was proposed by Anselone's theory of collectively compact operators (for more details, see the work by Anselone[31]). Anselone also described the condition for the convergence of the method (see the book by Anselone[32] for more details). Alselone's results were generalized for multidimensional problems in the work by Rak.[33] The main results are summed up in Sec. III A. There must be some special conditions for the kernel function, its approximation, and also for the type of the numerical integration rule.

A. Convergence conditions

Let us start with conditions for the kernel function. Suppose that the function $k(x,t)$ can be written as

$$k(x,t) = g(r(x,t))h(x,t), \quad (10)$$

where the function $h \in \mathscr{C}(D \times D)$, and where the function $g \in \mathscr{C}(0,\infty)$, is a positive non-increasing function with the limit

$$\lim_{t\to 0+} g(t) = \infty. \quad (11)$$

Let there exist a constant $c_D < \infty$ satisfying

$$\max_{x\in D} \int_{\{t,r(x,t)<R_D\}} g(r(x,t))dt \le c_D, \quad (12)$$

where

$$R_D = \max_{x,t\in D} r(x,t),$$

and let the limit

$$\lim_{v\to 0} \max_{x\in D} \int_{\{t,r(x,t)<v\}} g(r(x,t))dt = 0. \quad (13)$$

Let us have a positive decreasing sequence μ_n with its limit

$$\lim_{n\to\infty} \mu_n = 0. \quad (14)$$

Let us define the positive and non-increasing function $g_{\mu_n} \in \mathscr{C}[0,\infty)$ as

$$g_{\mu_n}(u) = \begin{cases} g(u) & \text{if } u \ge \mu_n, \\ g(\mu_n), & \text{if } u < \mu_n. \end{cases} \quad (15)$$

Finally, the bounded approximation $k_n(x,t)$ of the function $k(x,n)$ can be defined as

$$k_n(x,t) = g_{\mu_n}(r(x,t))h(x,t). \quad (16)$$

Let us continue with the integration rule assumptions. Suppose that the integration rule has positive weights and converges for all the continuous functions. Let us define the constant

$$\overline{w}_n = \max_{j=1,\ldots,n} w_j. \quad (17)$$

Let the sequence μ_n satisfies the condition

$$\mu_n^m \ge \rho^m \overline{w}_n, \quad (18)$$

where $0 < \rho < \infty$. Suppose that there exists a constant $\overline{\mu} < \infty$ satisfying

$$g(\mu_n)\overline{w}_n \le \overline{\mu}, \tag{19}$$

for all n. Finally, suppose that for all the positive, non-increasing functions $z \in \mathscr{C}[0,\infty)$ and $x \in D$, the inequality,

$$\sum_{j, r(x,x_j)\le\xi} w_j z(r(x,x_j)) \le cz(0)\overline{w}_n + c \int_{\{t, r(x,t)\le\xi\}} z(r(x,t))dt, \tag{20}$$

holds with the constants $c < \infty$ and $0 < \xi < \infty$.

From the description of the problem explained above, we can see that the error of the method will depend on the type of the numerical integration rule and the type of singularity of function $k(x,t)$. For the function $k(x,t)$, conditions given by Eqs. (10)–(14) are necessary. For the integration rule, conditions given by Eqs. (17)–(20) are necessary.

B. One dimensional test

To demonstrate the error behavior and to verify the theory outlined in Sec. III A, let us make a numerical experiment with Eq. (1) and the function

$$k(x,t) = |x-t|^{-\gamma}, \tag{21}$$

where $\gamma \in (0,1)$. Anselone[32] described the following conditions for the numerical integration rule. It needs to satisfy either the condition

$$\sum_{x_j\in E} w_j \le \frac{c}{n}, \quad E = [a,b) \text{ and } (a,b], \quad b-a \le \frac{1}{n}, \tag{22}$$

where

$$a, b \in [0,1],$$

or the condition

$$w_j, w_{j-1} \le c(x_j - x_{j-1}), \quad j = 2,\dots,n, \tag{23}$$

where $c < \infty$ is a constant independent of n. This is satisfied by all the compound numerical integration rules. The function given by Eq. (21) fulfills Eq. (10) with $h(x,t) = 1$ and $g(r) = r^{-\gamma}$. Analogously, the compactness of the operator $\mathscr{K}$ on $\mathscr{C}[0,1]$ is fulfilled. For approximation of the function $k(x,t)$, let us take function $k_n(x,t) = g_n(|x-t|)$ with

$$g_n(r) = g(r) \text{ when } r > \frac{1}{n} \text{ and } g_n(r) = g\left(\frac{1}{n}\right), \tag{24}$$

when

$$r \le \frac{1}{n}.$$

In the work by Rak,[33] the error estimate for the compound midpoint rule was proposed. All the results are featured in the following theorem.

TABLE I. Error behavior of the Nyström method with the compound midpoint rule with the exact solution e^x.

n	$\|y-y_n\|_\infty$	Ratio
20	0.001 681 00	3.83
40	0.000 437 55	3.84
80	0.000 142 16	3.08
160	0.000 048 21	2.95

Theorem 1. *Let Eq. (1) has solution y. Let the function $k(x,t)$ satisfies Eq. (10). Let the functions $h(x,t) \in \mathscr{C}([0,1]\times[0,1])$, $g(r) = r^{-\gamma}$ and let $\gamma \in (0,1)$. Let the numerical integration rule be a compound midpoint rule. Let the function g_n be as Eq. (24) and let the function k_n be as Eq. (16). Then, for a large enough n, there exist constants $\overline{C}$ and c_1 such that the error of the numerical solution y_n of Eq. (7) can be bounded by inequality given as*

$$\|y-y_n\| \le \overline{C}\left[\frac{2}{1-\gamma}\max_{x\in[0,1]}\mathscr{W}\left(h_x, \frac{1}{n}\right) + \frac{2c_1}{n^{1-\gamma}}\right], \tag{25}$$

where $\mathscr{W}$ is the modulus of continuity; function h_x is defined as

$$h_x(t) = y(t)h(x,t).$$

If $y \in \mathscr{C}^2[0,1]$ and $h(x,t) \in \mathscr{C}^2([0,1]\times[0,1])$, then there exists the constant c_2 such the error of the numerical solution y_n of Eq. (7) can be bounded by inequality given as

$$\|y-y_n\| \le \overline{C}\frac{c_2}{n^{2-\gamma}}. \tag{26}$$

The error of the numerical solution depends on the type of singularity and the error of the numerical integration. In this consequence, there should be no need to take the integration rule with an error better than $\mathscr{O}\left(\frac{1}{n^2}\right)$. That is why the compound midpoint rule was used in the theorem. The analogous theorem can be proven for other kernel functions and other integration rules.

Let us make an experiment with $\gamma = \frac{1}{2}$ and $h(x,t) = 1$. Let us choose $f(x)$ such that the integral equation given by Eq. (1) with kernel function $k(x,t)$ defined by Eq. (21) has the exact solution $y_e(x)$. The number n is equal to the number of node points in the compound rule. The "Ratio" columns show the ratio of successive errors.

TABLE II. Error behavior of the Nyström method with the compound midpoint rule with the exact solution $\sqrt{x}$.

n	$\|y-y_n\|_\infty$	Ratio
20	0.007 528 62	2.71
40	0.003 296 85	2.28
80	0.001 506 04	2.18
160	0.000 693 79	2.17

TABLE III. Error behavior of the Nyström method with the compound midpoint rule with the exact solution $\sqrt[4]{x}$.

n	$\|y - y_n\|_\infty$	Ratio
20	0.014 720 64	2.32
40	0.007 764 13	1.90
80	0.004 182 52	1.87
160	0.002 279 37	1.83

TABLE IV. Error behavior of the Nyström method with the compound Simpson rule with the exact solution e^x.

n	$\|y - y_n\|_\infty$	Ratio
20	0.001 090 00	3.09
40	0.000 361 47	3.02
80	0.000 121 86	2.96
160	0.000 041 68	2.92

All calculations we have done by the Maple software. The expected ratio should be $\sqrt{2^3} \approx 2,83$ if $y_e \in \mathscr{C}^2[0,1]$ and $h \in \mathscr{C}^2([0,1] \times [0,1])$. For the function $y_e = \sqrt{x}$, which is the Hölder continuous function with a constant $\frac{1}{2}$, the expected ratio is $\sqrt{2} \approx 1,41$. For the function $y_e = \sqrt[4]{x}$, which is the Hölder continuous function with a constant $\frac{1}{4}$, the expected ratio is $\sqrt[4]{2} \approx 1.19$.

From Tables I–III, we can see that the error behaves as it was expected. We can also see that the bound given by Eq. (25) is too pessimistic. If the function does not have continuous derivatives on the entire domain, the modulus of the continuity needs to be in the bound. Therefore, we cannot get better results.

TABLE V. Error behavior of the Nyström method with the compound Simpson rule with the exact solution $\sqrt{x}$.

n	$\|y - y_n\|_\infty$	Ratio
20	0.010 513 08	2.09
40	0.005 042 12	2.08
80	0.002 427 88	2.08
160	0.001 175 22	2.07

TABLE VI. Error behavior of the Nyström method with the compound Simpson rule with the exact solution $\sqrt[4]{x}$.

n	$\|y - y_n\|_\infty$	Ratio
20	0.050 644 11	1.75
40	0.028 873 58	1.75
80	0.016 500 29	1.75
160	0.009 475 77	1.74

TABLE VII. Error behavior comparison for different methods and exact solution e^x.

n	Product int.	NM midpoint	NM Simpson
20	0.001 461 6	0.001 681 0	0.001 090 0
40	0.000 367 1	0.000 437 5	0.000 361 5
80	0.000 095 1	0.000 142 1	0.000 121 9
160	0.000 022 1	0.000 048 2	0.000 041 7

TABLE VIII. Error behavior comparison for different methods and exact solution $\sqrt{x}$.

n	Product int.	NM midpoint	NM Simpson
20	0.032 205 4	0.007 528 6	0.010 513 1
40	0.012 621 6	0.003 296 9	0.005 042 1
80	0.006 076 0	0.001 506 0	0.002 427 9
160	0.002 903 4	0.000 693 8	0.001 175 2

The last fact for verification is if a better integration rule can improve the error behavior. Let us try the compound Simpson rule, which is of order $\mathcal{O}\left(\frac{1}{n^4}\right)$ for the same functions. From Tables IV–VI, it is clearly seen that there is no better error behavior.

Let us now compare the Nyström method with singularity subtraction with the product integration method described in the book by Atkinson.[29] The error for the same functions is displayed in Tables VII–IX. We can see that both methods show identical error behavior if the exact solution is the function with continuous derivatives. If the exact solution does not have continuous derivatives, the Nyström method has better behavior. The main goal is to measure the computing time. We can see in Table X that the Nyström method is much faster. This is viewed as the advantage for the application of the Nyström method in multidimensional problems.

TABLE IX. Error behavior comparison for different methods and exact solution $\sqrt[4]{x}$.

n	Product int.	NM midpoint	NM Simpson
20	0.112 030 9	0.014 720 6	0.050 644 1
40	0.059 568 3	0.007 764 1	0.028 873 6
80	0.034 186 4	0.004 182 5	0.016 500 3
160	0.019 320 3	0.002 279 4	0.009 475 8

TABLE X. Computing time for $y(x) = e^x$, Intel Core i5-2500@3.30GHz.

n	Product int. (s)	Nyström - midpoint (s)	Nyström - Simpson (s)
20	26.6	4.5	3.7
40	120.1	8.9	8.9
80	688.5	19.8	19.2

IV. INTEGRAL EQUATION FOR INDUCTION HEATING

Let us see Fig. 1, which shows the metal body $\mathbf{\Omega}_1$ heated by an inductor $\mathbf{\Omega}_2$. The equation for the Joule losses in the cuboid metal body $\mathbf{\Omega}_1 = \{(x_1, x_2, x_3), a \le x_1 \le b, c \le x_2 \le d, e \le x_3 \le f\}$ heated by a coil $\mathbf{\Omega}_2$ (reported in the study by Solin *et al.*[34]) is

$$\omega_J(x) = \frac{1}{\gamma} J_e(x)\overline{J_e(x)}, \tag{27}$$

where

$$\begin{aligned} J_e(x) \;=\; & \sqrt{[\mathrm{Re}J_{eddy,x_1}(x)]^2 + [\mathrm{Re}J_{eddy,x_2}(x)]^2 + [\mathrm{Re}J_{eddy,x_3}(x)]^2} \\ & + \imath\sqrt{[\mathrm{Im}J_{eddy,x_1}(x)]^2 + [\mathrm{Im}J_{eddy,x_2}(x)]^2 + [\mathrm{Im}J_{eddy,x_3}(x)]^2}, \end{aligned}$$

and $\overline{J_e(x)}$ is a complex conjugate to $J_e(x)$. $J_{eddy} = (J_{eddy,x_1}, J_{eddy,x_2}, J_{eddy,x_3})$ denotes the eddy current of the density phasor. It is a solution of an integral equation, described in Sec. III B, in the form of

$$\imath J_{eddy}(x) - \kappa(x) \int_{\Omega_1} \frac{J_{eddy}(t)}{r(x,t)} dt_1 dt_2 dt_3 = \kappa(x) I_{ext} \int_{\Omega_2} \frac{dl(s)}{r(x,s)}, \tag{28}$$

where

$$\kappa(x) = \frac{\omega\gamma(T(x))\mu_0}{4\pi},$$

where x and t are the points in the heated body, s is a point in the inductor, r is the Euclidean distance, and $\imath$ is a complex unit. The constant μ_0 is the permeability of vacuum. The $dl(s)$ denotes a length element of the inductor. The constant ω represents an angular frequency of the field current. The constant γ stands for the electrical conductivity of the metal. I_{ext} is the field current carried by the inductor. Finally, $T(x)$ represents a temperature in the body at point x. Equation (28) can be obtained from Eq. (1) by putting $\lambda = 1$, $k(x,t) = -\imath\kappa(x) r(x,t)^{-1}$ and

$$f(x) = -\imath\kappa(x) I_{ext} \int_{\Omega_2} \frac{dl(s)}{r(x,s)}.$$

We can use sphere coordinates to prove that the appropriate operator given by Eq. (3) is a compact operator on $\mathscr{C}(\mathbf{\Omega}_1)$. For the existence and uniqueness of the solution of Eq. (28), we can use the Fredholm alternative. We need to prove that 1 is not an eigenvalue of the operator $\mathscr{K}$. This can be done by a construction of a $\frac{1}{\kappa}$-weighted inner product. The operator $\mathscr{K}$ can be proved to be antisymmetric, which implies that $\lambda = 1$ is not its eigenvalue and Eq. (28) has a unique solution. For a numerical solution, we will use the described Nyström method with the singularity subtraction with the compound mid-cuboid rule for the numerical integration. The following theorem was proved in the work by Rak.[33]

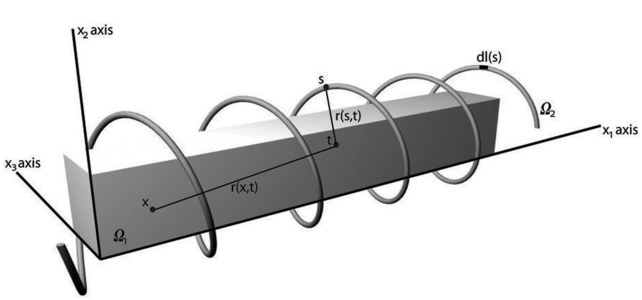

FIG. 1. Scheme of induction heating.

Theorem 2. *Let us have a cuboid $D = \{(x_1, x_2, x_3), a \le x_1 \le b, c \le x_2 \le d, e \le x_3 \le f\}$. Let the cuboid be divided by $n_1 n_2 n_3$ subcuboids (n_1 in x_1 direction, n_2 in x_2 direction, and n_3 in x_3 direction). Let $h_1 = (b-a)n_1^{-1}$, $h_2 = (d-c)n_2^{-1}$, and $h_3 = (f-e)n_3^{-1}$. Suppose that there exist constants α, β satisfying $1 \le \beta \le \alpha < \infty$ such that $h_1 = \alpha h_3$ and $h_2 = \beta h_3$. Then, for the compound mid-point integration rule, there exist constants c and ξ such that Eq. (20) holds.*

From the tests in Sec. III B, we identified that there is no need to take the numerical integration rule with better error behavior. With Theorem 2, Eq. (20) is satisfied. Setting $h(x,t) = -\imath\kappa(x)$ and $g(u) = u^{-1}$, the function $k(x,t)$ can be written as Eq. (10). Its bounded approximation given by Eq. (16) can be defined as

$$k_n(x,t) = \frac{-\imath\kappa(x)}{r_n(x,t)}, \tag{29}$$

where

$$r_n(x,t) = \begin{cases} r(x,t) & \text{if } r(x,t) \ge \mu_n, \\ \mu_n & \text{if } r(x,t) < \mu_n, \end{cases}$$

and

$$\mu_n = \sqrt[3]{\frac{(b-a)(d-c)(f-e)}{n}}.$$

We can prove that the kernel function $k(x,t)$ and its approximation defined by Eq. (29) fulfill conditions given by Eqs. (10)–(14). We can also prove that the compound mid-cuboid rule and the kernel function fulfill the conditions given by Eqs. (17)–(20). For more details, please see the work by Rak.[33] Considering all these facts, the Nyström method with a singularity subtraction converges for the compound mid-point rule.

Example 1. Let us compute the Joule losses in a cuboid body with a size of $0.15 \times 0.01 \times 0.01$ m3. *The body is heated with a stationary inductor. The heating process starts at room temperature* (20 °C). *Coil plays a role of an inductor. The coil turns around the heated body in the x_1-direction in six loops. The coil has a radius of* 0.015 m. *The current in the coil is* 500 A *with a frequency of* 150 kHz. *The coil is* 0.15 m *in length. The cuboid body is divided by 75 elements in the x_1 direction, 10 elements in the x_2 direction, and 10 elements in the x_3 direction. The Joule losses in the body at the x_1 axis with $x_2 = -0.004$ are displayed for different x_3 coordinates in Fig. 2. The blue color indicates $x_3 = -0.004$, the red color indicates $x_3 = 0$, and the black color indicates $x_3 = 0.004$. The Joule losses in the body at the x_1 axis with $x_2 = 0$ axis are displayed in Fig. 3 in the same way.*

All the calculations were performed in Matlab. The computation of $F(x_i)$ was realized by Matlab's method *quad*. This method uses the adaptive Simpson quadrature. The improper integral was computed analytically.

V. THE NON-STATIONARY TEMPERATURE DISTRIBUTION

The non-stationary distribution of the temperature $T(x,t)$ at a point x and time t in the metal body is described by a partial differential equation of the parabolic type, i.e.,

$$\operatorname{div}\left[\lambda(T(x,t))\operatorname{grad}T(x,t)\right] = \rho(T(x,t))c(T(x,t))\frac{\partial T(x,t)}{\partial t} - \omega(x,t), \tag{30}$$

where $\lambda = \lambda(T(x,t))$ denotes the thermal conductivity, $\rho = \rho(T(x,t))$ represents the specific mass of the material, $c = c(T(x,t))$ stands for the specific heat, and $\omega(x,t)$ is the specific Joule losses given by Eq. (27) at a time t.

The boundary condition along the whole surface of the body reads as

$$-\lambda(T(x,t))\frac{\partial T(x,t)}{\partial n} = \alpha(T(x,t) - T_{ext}), \tag{31}$$

where α denotes the coefficient of the convective heat transfer, T_{ext} is the temperature of the surrounding medium, and n represents the direction of the outward normal.

Let us use the finite difference method for the numerical solution of Eq. (30). Since the thermal conductivity is a parameter that depends on the temperature, we can rewrite Eq. (30) in the form of

$$\frac{\partial T(x,t)}{\partial t} = \frac{1}{\rho(T(x,t))c(T(x,t))}\cdot\left[\lambda(T(x,t))\left(\frac{\partial^2 T(x,t)}{\partial x_1^2} + \frac{\partial^2 T(x,t)}{\partial x_2^2} + \frac{\partial^2 T(x,t)}{\partial x_3^2}\right) + \omega(x,t)\right]. \tag{32}$$

Let the coordinates of the node point be

$$(x_{1_i}, x_{2_j}, x_{3_k}), \quad i = 1,\ldots,n_1, \quad j = 1,\ldots n_2, \quad k = 1,\ldots,n_3.$$

With the notations

$$\begin{aligned} x_{i,j,k} &= x_{1_i}, x_{2_j}, x_{3_k}, \\ T_{i,j,k}(t) &= T(x_{i,j,k}, t), \\ \omega_{i,j,k}(t) &= \omega(x_{i,j,k}, t), \end{aligned}$$

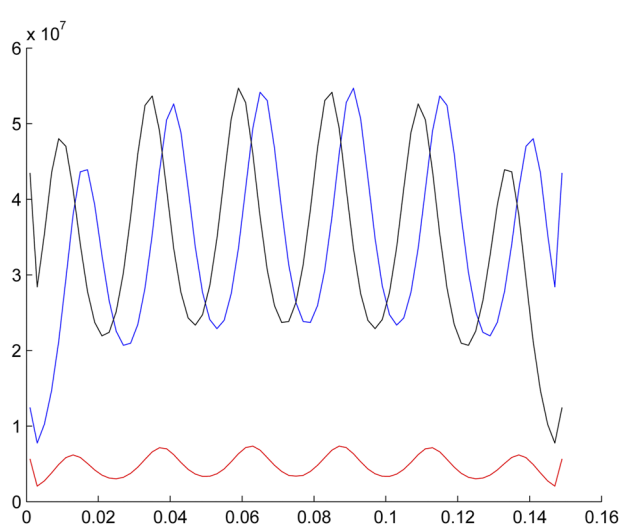

FIG. 2. Induction heating example—Joule losses.

the x_1, x_2, and x_3 derivatives are approximated by

$$\begin{aligned} \frac{\partial^2 T(x,t)}{\partial x_1^2} &\approx \frac{T_{i+1,j,k}(t) - 2T_{ijk}(t) + T_{i-1,j,k}(t)}{h_1^2}, \\ \frac{\partial^2 T(x,t)}{\partial x_2^2} &\approx \frac{T_{i,j+1,k}(t) - 2T_{ijk}(t) + T_{i,j-1,k}(t)}{h_2^2}, \\ \frac{\partial^2 T(x,t)}{\partial x_3^2} &\approx \frac{T_{i,j,k+1}(t) - 2T_{ijk}(t) + T_{i,j,k-1}(t)}{h_3^2}. \end{aligned} \tag{33}$$

Now, let us approximate the derivative by the difference in the boundary condition given by Eq. (31) to define T_{ijk} for $i = 0$, $i = n_1 + 1$, $j = 0$, $j = n_2 + 1$, $k = 0$, and $k = n_3 + 1$. Thus,

$$\begin{aligned} T_{0,j,k}(t) &= T_{1,j,k} - \frac{h_1\alpha}{\lambda(T_{1,j,k}(t))}(T_{1,j,k} - T_{ext}), \\ T_{n_1+1,j,k}(t) &= T_{n_1,j,k} - \frac{h_1\alpha}{\lambda(T_{n_1,j,k}(t))}(T_{n_1,j,k} - T_{ext}), \\ T_{i,0,k}(t) &= T_{i,1,k} - \frac{h_2\alpha}{\lambda(T_{i,1,k}(t))}(T_{i,1,k} - T_{ext}), \\ T_{i,n_2+1,k}(t) &= T_{i,n_2,k} - \frac{h_2\alpha}{\lambda(T_{i,n_2,k}(t))}(T_{i,n_2,k} - T_{ext}), \\ T_{i,j,0}(t) &= T_{i,j,1} - \frac{h_3\alpha}{\lambda(T_{i,j,1}(t))}(T_{i,j,1} - T_{ext}), \\ T_{i,j,n_3+1}(t) &= T_{i,j,n_3} - \frac{h_3\alpha}{\lambda(T_{i,j,n_3}(t))}(T_{i,j,1n_3} - T_{ext}). \end{aligned} \tag{34}$$

Let us define the time step Δt to approximate the time derivative by

$$\frac{\partial T(x,t)}{\partial t} \approx \frac{T(x,t+\Delta t) - T(x,t)}{\Delta t}. \tag{35}$$

From Eqs. (32)–(35), we arrive at the numerical formula for the temperature evolution, i.e.,

$$T_{i,j,k}(t+\Delta t) = T_{i,j,k}(t) + \frac{\Delta t}{\rho(T_{i,j,k}(t))c(T_{i,j,k}(t))} \cdot \left[\lambda(T_{ijk}(t))\left(\frac{T_{i+1,j,k}(t) - 2T_{i,j,k}(t) + T_{i-1,j,k}(t)}{h_1^2} + \frac{T_{i,j+1,k}(t) - 2T_{i,j,k}(t) + T_{i,j-1,k}(t)}{h_2^2} + \frac{T_{i,j,k+1}(t) - 2T_{i,j,k}(t) + T_{i,j,k-1}(t)}{h_3^2}\right) + \omega_{i,j,k}(t)\right].$$

Joule losses need to be updated when the time changes. The whole calculation is started with an initial condition. It is the starting temperature of the body, which is equal to the temperature of the air of the surrounding medium. Let us finish this section with examples—Figures of the temperature distribution in the metal body in different situations. The unit for temperature distribution is Celsius degree.

Example 2. Let us now compute the temperature distribution in the metal body. Let us have the same situation as in Example 1.

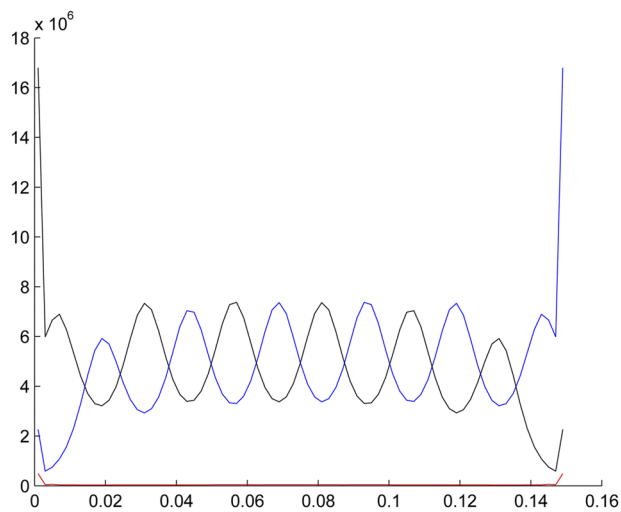

FIG. 3. Induction heating example—Joule losses.

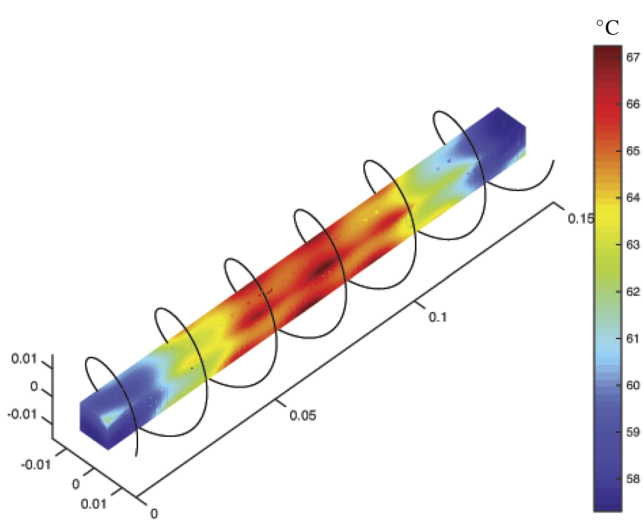

FIG. 4. Size: 0.15 × 0.01 × 0.01 m^3. Time: t = 10 s. Number of loops: 6. Current: 500 A. Frequency of 150 kHz.

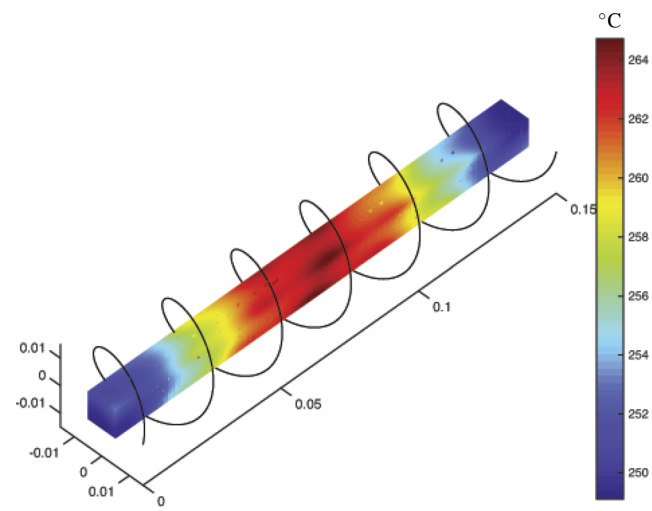

FIG. 5. Size: 0.15 × 0.01 × 0.01 m^3. Time: t = 60 s. Number of loops: 6. Current: 500 A. Frequency of 150 kHz.

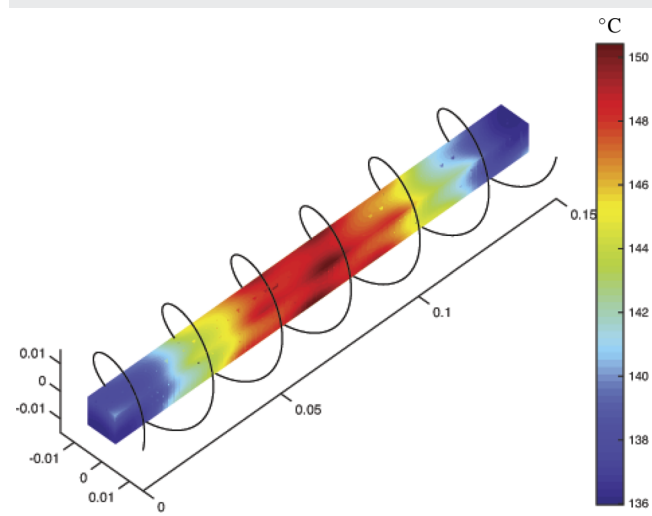

FIG. 6. Size: 0.15 × 0.01 × 0.01 m^3. Time: t = 30 s. Number of loops: 6. Current: 500 A. Frequency of 150 kHz.

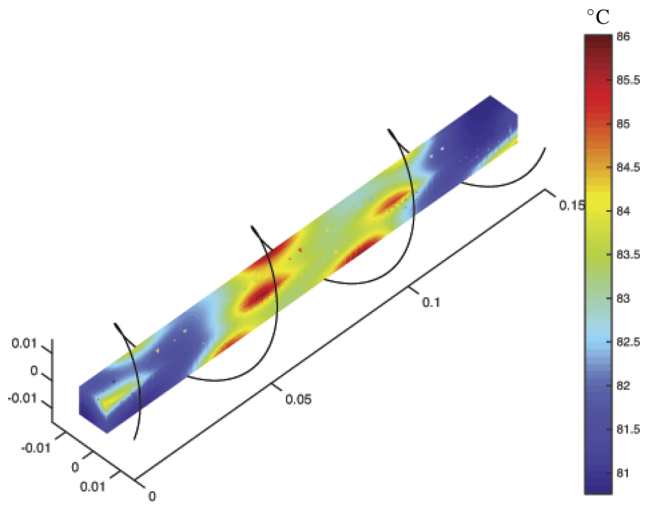

FIG. 7. Size: 0.15 × 0.01 × 0.01 m^3. Time: t = 60 s. Number of loops: 3. Current: 500 A. Frequency of 150 kHz.

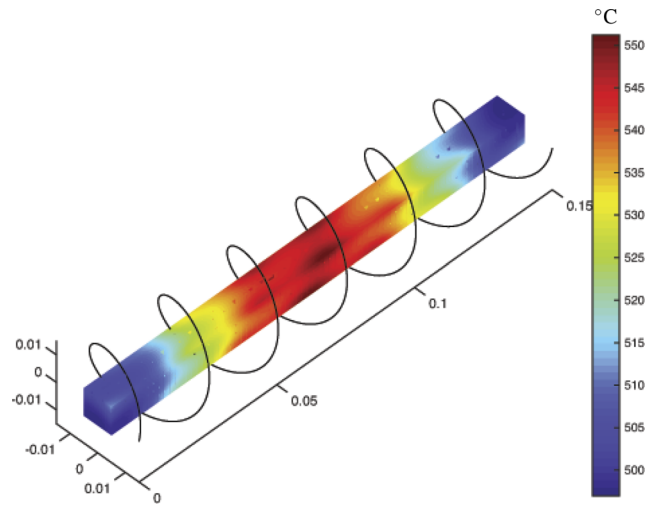

FIG. 9. Size: 0.15 × 0.01 × 0.01 m^3. Time: t = 60 s. Number of loops: 6. Current: 1000 A. Frequency of 150 kHz.

Figure 4 shows the temperature distribution in the body at a time of 10 s. *Figure 5 shows the temperature distribution in the body at a time of* 60 s.

To see the dependence of the parameters, let us show the example with different parameters.

Example 3. Let us now compute the temperature distribution in the metal body. Let us have the same situation as in Example 2 with one parameter change. Figure 6 shows the temperature distribution at 30 s *with original parameters. Figure 7 shows the situation when the coil rotates over the heating body at three loops. Figure 8 shows the situation if the size of the body is* 0.15 × 0.005 × 0.005 m^3. *Figure 9 shows the situation if the coil has an exciting current of* 1000 A. *Finally, Fig. 10 shows the situation when the angular frequency is 300 kHz.*

We can see that the temperature changed as was excepted. Using this method, it is also very easy to implement body or the inductor movement. The only change is that the right hand side of

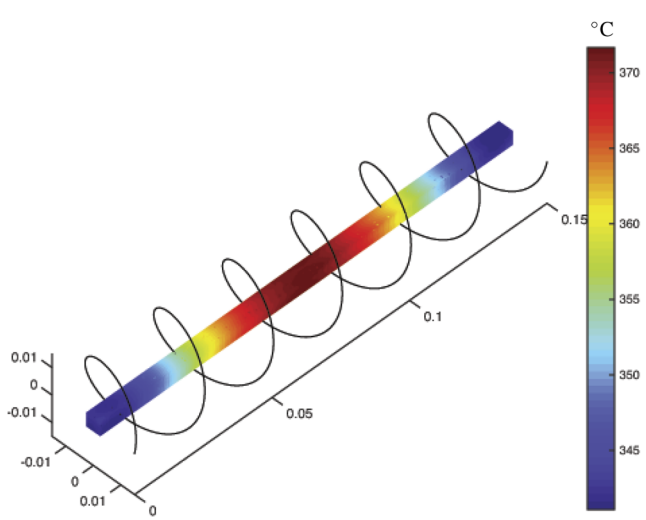

FIG. 8. Size: 0.15 × 0.005 × 0.005 m^3. Time: t = 60 s. Number of loops: 6. Current: 500 A. Frequency of 150 kHz.

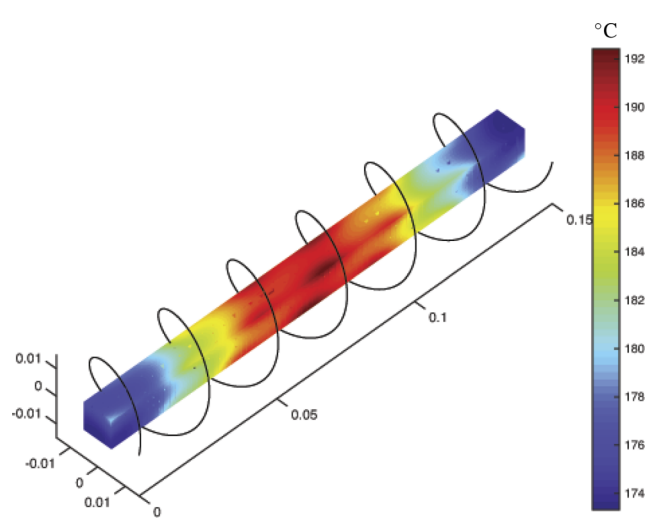

FIG. 10. Size: 0.15 × 0.01 × 0.01 m^3. Time: t = 60 s. Number of loops: 6. Current: 500 A. Frequency of 300 kHz.

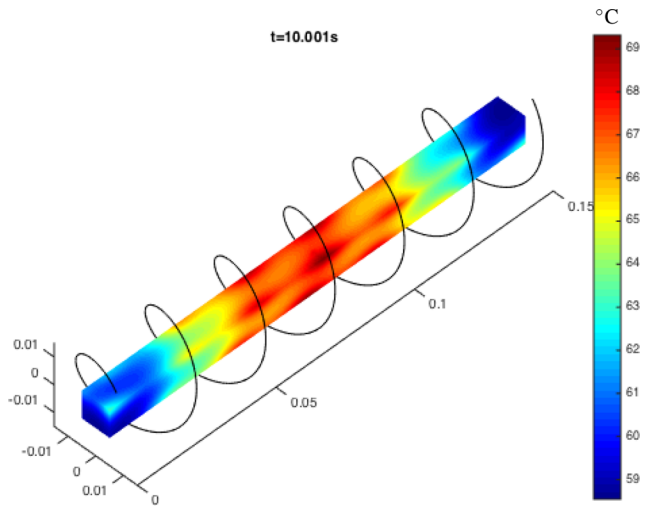

FIG. 11. Size: 0.15 × 0.01 × 0.01 m^3. Time: t = 10 s. Number of loops: 6. Current: 500 A. Frequency of 150 kHz. Rotating coil.

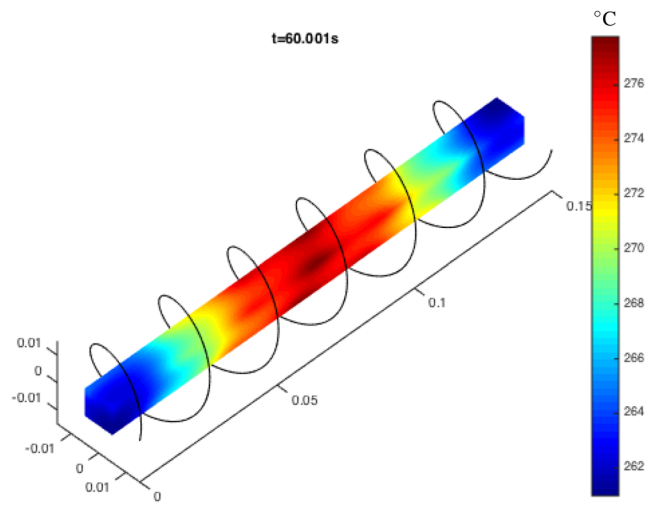

FIG. 13. Size: 0.15 × 0.01 × 0.01 m^3. Time: t = 60 s. Number of loops: 6. Current: 500 A. Frequency of 150 kHz. Rotating coil.

Eq. (28) depends on the time. What happens due to the movement of the inductor is shown in the last example.

Example 4. Let us have the same situation as in Example 2. The coil rotates around the body. The time needed to complete one rotation is 60 s. *The cuboid is partitioned by 75 elements in the x_1 direction, and 10 elements in the x_2 and x_3 directions.* Figures 11 and 13 *display the temperature distribution on the surface of the body after 10, 30, and 60 s, respectively.*

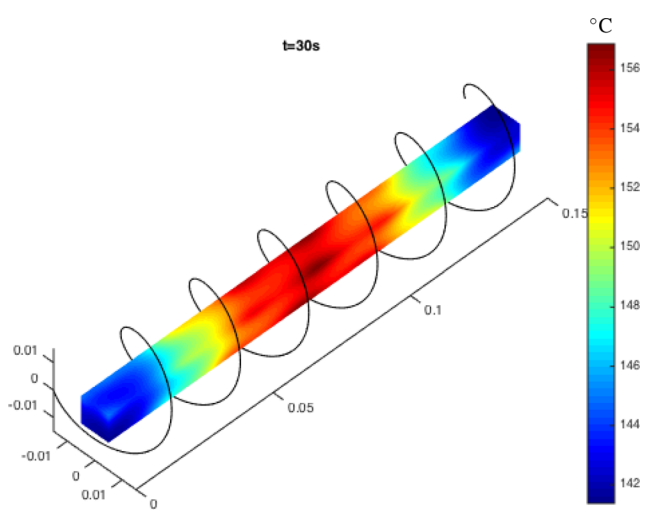

FIG. 12. Size: 0.15 × 0.01 × 0.01 m^3. Time: t = 30 s. Number of loops: 6. Current: 500 A. Frequency of 150 kHz. Rotating coil.

VI. CONCLUSION

In this work, we have presented an innovative approach for the mathematical modeling of the induction heating process. The developed procedure involving Fredholm integral equations of the second kind with a singular kernel and the Nyström method was found to show promising performance in terms of the computation time. Furthermore, the error features of the Nyström method with the singularity subtraction were studied, and convergence conditions were identified.

The Nyström method, adopted in the proposed computational algorithm, shows more advantages compared to other approaches used in induction heating modeling. Since a detailed knowledge of the 3D-magnetic field is not necessary, it is easy to implement the body or inductor movement, extending thus the portfolio of experimental setups (e.g., spatial arrangements of a coil and heated object, types of induction heating processes) to model efficiently. As most computing time is spent on the computation of the eddy current density, the Nyström method can rapidly reduce the time demand of the algorithm. Although special conditions for the kernel function and the integration rule are needed, the method shows lower computing times well competing with those of traditional finite-element based routines. The time needed for computation is lowered due to the convenient mathematical structure of the problem when the integrals are present only in the diagonal elements of the matrix in Eq. (7) and other elements are easily calculated. If we compare the computing time on Windows 7 operating system with Intel Core i5 and 4GB RAM, we get ~2 min for the Nyström method and ~12 min for the piecewise constant collocation.

Although only Joule losses were considered in the modeling of the magnetic induction heating, the suggested approach offers to add other heat contributions, such as those originating from hysteresis phenomena. As shown earlier in the works by Wetzel and Fink[35,36] and recently in the study by Martin *et al.*,[37] the dissipation of heat due to hysteresis losses upon placing a ferromagnetic material into an alternating magnetic field can be expressed by the heating rate

equations. Since the hysteresis heat results from the reorientation of the magnetic moments in the material in the external magnetic field, it can be treated independently on the Joule losses, thus as an additive term. This could give simulation results closer to the experimental observations, especially in the cases of designing the magnetic susceptors and optimization of their performance.[37]

Finally, the method, proposed here, can be adopted for other physical problems where the partial differential equations can be transformed into the Fredholm integral equations of the second kind. The only condition is that the possible singularity can be subtracted. Thus, on a general level, the presented algorithm shows the potential to be used for other physical processes that need to be modeled (e.g., heat conduction). Fredholm's integral equation is transformed into a system of linear equations. The big advantage is that the matrix of the system can be computed with low computing time because only the diagonal elements of the matrix are integrals, which are needed to be calculated.

AUTHOR DECLARATIONS

Conflict of Interest

The authors have no conflicts to disclose.

Author Contributions

J. Rak: Data curation (equal); Formal analysis (equal); Software (equal). **J. Tucek**: Formal analysis (equal); Validation (equal).

DATA AVAILABILITY

The data that support the findings of this study are available from the corresponding author upon reasonable request.

REFERENCES

[1] V. I. Rudnev, D. Loveless, R. Cook, and M. Black, *Handbook of Induction Heating* (CRC Press, 2002).

[2] R. C. O'Handley, *Modern Magnetic Materials: Principles and Applications* (John Wiley, 2000).

[3] K. F. Wang, S. Chandrasekar, and H. T. Y. Yang, "Finite element simulation of induction heat treatment," J. Mater. Eng. Perform. **1**(1), 97–112 (1992).

[4] K. F. Wang, S. Chandrasekar, and H. T. Y. Yang, "Finite element simulation of moving induction heat treatment," J. Mater. Eng. Perform. **4**(4), 460–473 (1995).

[5] L. I. Faerman, V. I. Luzgin, A. Y. Petrov, and S. A. Rachkov, "Highly efficient induction heating units for metallurgy and machine construction," Metallurgist **41**(5–6), 191–193 (1997).

[6] S.-C. Nian, S.-W. Tsai, M.-S. Huang, R.-C. Huang, and C.-H. Chen, "Key parameters and optimal design of a single-layered induction coil for external rapid mold surface heating," Int. Commun. Heat Mass Transfer **57**, 109–117 (2014).

[7] B. J. Knauf, D. P. Webb, C. Liu, and P. P. Conway, "Low frequency induction heating for the sealing of plastic microfluidic systems," Microfluid. Nanofluid. **9**(2–3), 243–252 (2010).

[8] S. Zinn and S. L. Semiatin, *Elements of Induction Heating: Design, Control, and Applications* (ASM International, 1988).

[9] B. Ducharne, M. Q. Le, G. Sebald, P. J. Cottinet, D. Guyomar, and Y. Hebrard, "Characterization and modeling of magnetic domain wall dynamics using reconstituted hysteresis loops from Barkhausen noise," J. Magn. Magn. Mater. **432**, 231–238 (2017).

[10] A. K. Gupta and M. Gupta, "Synthesis and surface engineering of iron oxide nanoparticles for biomedical applications," Biomaterials **26**(18), 3995–4021 (2005).

[11] C. S. S. R. Kumar and F. Mohammad, "Magnetic nanomaterials for hyperthermia-based therapy and controlled drug delivery," Adv. Drug Delivery Rev. **63**(9), 789–808 (2011).

[12] K. Hola, Z. Markova, G. Zoppellaro, J. Tucek, and R. Zboril, "Tailored functionalization of iron oxide nanoparticles for MRI, drug delivery, magnetic separation and immobilization of biosubstances," Biotechnol. Adv. **33**(6), 1162–1176 (2015).

[13] I. Raouf, S. Khalid, A. Khan, J. Lee, H. S. Kim, and M.-H. Kim, "A review on numerical modeling for magnetic nanoparticle hyperthermia: Progress and challenges," J. Therm. Biol. **91**, 102644 (2020).

[14] I. Doležel, P. Kropík, and B. Ulrych, "Induction heating of thin metal plates in time-varying external magnetic field solved as nonlinear hard-coupled problem," Appl. Math. Comput. **219**(13), 7159–7169 (2013).

[15] E. Rapoport and Y. Pleshivtseva, *Optimal Control of Induction Heating Processes* (CRC Press, 2007).

[16] A. Gagnoud, "Three-dimensional integral method for modeling electromagnetic inductive processes," IEEE Trans. Magn. **40**(1), 29–36 (2004).

[17] U. Ludtke and D. Schulze, "Numerical simulation of continuous induction steel bar end heating with material properties depending on temperature and magnetic field," IEEE Trans. Magn. **34**(5), 3110–3113 (1998).

[18] J. Nerg, K. Tolsa, P. Silventoinen, J. Partanen, and J. Pyrhonen, "A dynamic model for the simulation of induction heating devices," IEEE Trans. Magn. **35**(5), 3592–3594 (1999).

[19] H. Kawaguchi, M. Enokizono, and T. Todaka, "Thermal and magnetic field analysis of induction heating problems," J. Mater. Process. Technol. **161**(1–2), 193–198 (2005).

[20] F. Mach, P. Kus, P. Karban, and I. Dolezel, "Optimization of the system for induction heating of nonmagnetic cylindrical billets in rotating magnetic field produced by permanent magnets," Computing **95**(1), 537–552 (2013).

[21] J. Chovan and M. Slodička, "Induction hardening of steel with restrained Joule heating and nonlinear law for magnetic induction field: Solvability," J. Comput. Appl. Math. **311**, 630–644 (2017).

[22] M. Slodička and J. Chovan, "Solvability for induction hardening including nonlinear magnetic field and controlled Joule heating," Appl. Anal. **96**(16), 2780–2799 (2017).

[23] K. Gürlebeck, A. Hommel, and A. Legatiuk, "Numerical modelling of an induction heating problem," AIP Conf. Proc. **2116**, 160002 (2019).

[24] T. Fu, J. Xu, and Z. Hui, "Analysis of induction heating temperature field of plain weave CFRP based on finite element meso model," Appl. Compos. Mater. **28**(1), 149–163 (2021).

[25] P. Cui, W. Zhu, H. Ji, H. Chen, C. Hang, and M. Li, "Analysis and optimization of induction heating processes by focusing the inner magnetism of the coil," Appl. Energy **321**, 119316 (2022).

[26] V. C. Le, M. Slodička, and K. Van Bockstal, "Existence of a weak solution to a nonlinear induction hardening problem with Leblond–Devaux model for a steel workpiece," Commun. Nonlinear Sci. Numer. Simul. **107**, 106156 (2022).

[27] V. Geza, M. Scepanskis, R. Vilums, and A. Eimuss, "Potential of open source simulation tools for induction heating," IOP Conf. Ser.: Mater. Sci. Eng. **424**, 012066 (2018).

[28] K. Roppert, F. Toth, and M. Kaltenbacher, "Simulating induction heating processes using harmonic balance FEM," COMPEL - Int. J. Comput. Math. Electr. Electron. Eng. **38**(5), 1562–1574 (2019).

[29] K. E. Atkinson, *The Numerical Solution of Integral Equations of the Second Kind* (Cambridge University Press, 1997).

[30] L. V. Kantorovich and V. I. Krylov, *Approximate Methods of Higher Analysis* (Interscience, 1958).

[31] P. M. Anselone, *Collectively Compact Operator Approximation Theory and Applications to Integral Equations* (Prentice-Hall, 1971).

[32] P. M. Anselone, "Singularity subtraction in the numerical solution of integral equations," J. Aust. Math. Soc. (Ser. B) **22**, 408–418 (1981).

[33]J. Rak, "Numerical solution of a Fredholm integral equation of the second kind related to induction heating," Ph.D. thesis, Charles University Prague, 2012.
[34]P. Solin, I. Dolezel, M. Skopek, and B. Ulrych, "Induction heating of thin slabs in nonmagnetic media," in *Scientific Computing in Electrical Engineering*, Lecture Notes in Computational Science and Engineering (Springer, 2001), Vol. 18, pp. 143–146.
[35]E. D. Wetzel and B. K. Fink, "Feasibility of magnetic particle films for Curie temperature-controlled processing of composite materials," Report No. ARL-TR-2431, U.S. Army Research Laboratory, Aberdeen Proving Ground, MD, 2001.
[36]E. D. Wetzel and B. K. Fink, "Adherend thermal effects during bonding with inductively heated films," Report No. ARL-TR-2461, U.S. Army Research Laboratory, Aberdeen Proving Ground, MD, 2001.
[37]R. G. Martin, C. Johansson, J. R. Tavares, and M. Dubé, "Material selection methodology for an induction welding magnetic susceptor based on hysteresis losses," Adv. Eng. Mater. **24**(3), 2100877 (2022).